



저작자표시-비영리-변경금지 2.0 대한민국

이용자는 아래의 조건을 따르는 경우에 한하여 자유롭게

- 이 저작물을 복제, 배포, 전송, 전시, 공연 및 방송할 수 있습니다.

다음과 같은 조건을 따라야 합니다:



저작자표시. 귀하는 원저작자를 표시하여야 합니다.



비영리. 귀하는 이 저작물을 영리 목적으로 이용할 수 없습니다.



변경금지. 귀하는 이 저작물을 개작, 변형 또는 가공할 수 없습니다.

- 귀하는, 이 저작물의 재이용이나 배포의 경우, 이 저작물에 적용된 이용허락조건을 명확하게 나타내어야 합니다.
- 저작권자로부터 별도의 허가를 받으면 이러한 조건들은 적용되지 않습니다.

저작권법에 따른 이용자의 권리는 위의 내용에 의하여 영향을 받지 않습니다.

이것은 [이용허락규약\(Legal Code\)](#)을 이해하기 쉽게 요약한 것입니다.

[Disclaimer](#)

**Master's Thesis**

**석사 학위논문**

**Synthesis, Characterization and Reactivity of a  
Mononuclear Nickel(II)-Borohydride Complex**

Hyeonwoo Tak( 탁 현 우 卓 炫 佑)

Department of  
Emerging Materials Science

DGIST

2016

**Master's Thesis**

**석사 학위논문**

**Synthesis, Characterization and Reactivity of a  
Mononuclear Nickel(II)-Borohydride Complex**

Hyeonwoo Tak( 탁 현 우 초炫佑)

Department of  
Emerging Materials Science

DGIST

2016

# Synthesis, Characterization and Reactivity of a Mononuclear Nickel(II)-Borohydride Complex

Advisor: Professor Jaeheung Cho

Co-Advisor: Professor Hyun-Chul Kim

by

Hyeonwoo Tak

Department of Emerging Materials Science

A thesis submitted to the faculty of DGIST in partial fulfillment of the requirements for the degree of Master of Science, in the Department of Emerging Materials Science. The study was conducted in accordance with Code of Research Ethics.

05. 27. 2016

Approved by

Professor Jaeheung Cho      (Signature)  
(Advisor)

Professor Hyun-Chul Kim      (Signature)  
(Co-Advisor)

---

1) Declaration of Ethical Conduct in Research: I, as a graduate student of DGIST, hereby declare that I have not committed any acts that may damage the credibility of my research. These include, but are not limited to: falsification, thesis written by someone else, distortion of research findings or plagiarism. I affirm that my thesis contains honest conclusions based on my own careful research under the guidance of my thesis advisor.

# Synthesis, Characterization and Reactivity of a Mononuclear Nickel(II)-Borohydride Complex

Hyeonwoo Tak

Accepted in partial fulfillment of the requirements for the degree of Master of Science.

05. 27. 2016

Head of Committee 조 재 흥 (인)

Prof. Jaeheung Cho

Committee Member 김 현 철 (인)

Prof. Hyun-Chul Kim

Committee Member 정 낙 천 (인)

Prof. Nak Cheon Jeong

## Abstract

A nickel(II)-borohydride complex bearing a macrocyclic tridentate N-donor ligand,  $[\text{Ni}(\text{Me}_3\text{-TACN})(\text{BH}_4)(\text{CH}_3\text{CN})]^+$  ( $\text{Me}_3\text{-TACN}$  = 1,4,7-trimethyl-1,4,7-triazacyclononane), was prepared, isolated, and characterized by various physicochemical methods, including UV-vis, ESI-MS, IR and X-ray analyses. The structural and spectroscopic characterization clearly shows that the borohydride ligand is bound to the high-spin nickel(II) center in an  $\eta^2$ -manner. Density functional theory calculations provided geometric information of **2**, showing that the  $\eta^2$ -binding of borohydride to the nickel center is more favorable than the  $\eta^3$ -binding mode in  $\text{CH}_3\text{CN}$ . The complex is paramagnetic with an effective magnetic moment of  $2.9 \mu_{\text{B}}$  consistent with a  $d^8$  high-spin system.

The reactivity of the high-spin nickel(II)-borohydride complex was examined in dehalogenation with numerous halocarbons. A kinetic isotope effect value of 1.7 was observed in the dehalogenation of  $\text{CHCl}_3$  by the nickel(II)-borohydride complex. Kinetic studies and isotopic labeling experiments implicate that hydride ion or hydrogen atom transfer from the borohydride group is the rate determining step. The positive Hammett  $\rho$  value of 1.2, obtained in the reactions of  $[\text{Ni}(\text{Me}_3\text{-TACN})(\text{BH}_4)(\text{CH}_3\text{CN})]^+$  and *para*-substituted benzoyl chloride, indicates that the dehalogenation by the nickel(II)-borohydride species occurs via a nucleophilic reaction.

**Keywords:** High-spin nickel(II)-borohydride complex, dehalogenation,

# Contents

Abstract.....	i
List of contents.....	ii
List of tables.....	iv
List of figures.....	v

## I . Introduction

1.1 Motivation.....	1
1.2 Previous work.....	1
1.3 This work.....	2

## II . Results and discussion

2.1 Nickel(II) precursor complex.....	3
2.2 Nickel(II)–borohydride complex and characterization.....	5
2.3 Reactivity.....	12
2.4 Density functional theory results.....	19

## III. Conclusions

3.1 Conclusions.....	27
----------------------	----

## IV. Experimental section

4.1 Materials.....	28
4.2 Physical methods.....	28
4.3 Syntheses.....	29
4.3.1 [Ni(Me <sub>3</sub> -TACN)(CH <sub>3</sub> CN) <sub>2</sub> ](ClO <sub>4</sub> ) <sub>2</sub> ( <b>1</b> -(ClO <sub>4</sub> ) <sub>2</sub> ).....	29
4.3.2 [Ni(Me <sub>3</sub> -TACN)(BH <sub>4</sub> )(CH <sub>3</sub> CN)](BPh <sub>4</sub> ) ( <b>2</b> -(BPh <sub>4</sub> )).....	29
4.4 X-ray crystallography.....	30
4.5 Reactivity.....	31
4.6 Computational details.....	31

## List of tables

Table 1. Crystal data and structure refinements for <b>1</b> -(BPh <sub>4</sub> ) <sub>2</sub> and <b>2</b> -(BPh <sub>4</sub> ).....	10
Table 2. Selected bond distance (Å) and angles (°) for <b>1</b> -(BPh <sub>4</sub> ) <sub>2</sub> and <b>2</b> -(BPh <sub>4</sub> ).....	11
Table 3. Coordinates in xyz-format.....	21

## List of figures

Fig. 1 (a) UV-vis spectrum of <b>1</b> in acetonitrile (red) and the reflectance spectrum of a powdered sample of <b>1</b> (black, intensity scale is arbitrary).....	4
Fig. 1 (b) X-ray structure of the $[\text{Ni}(\text{Me}_3\text{-TACN})(\text{CH}_3\text{CN})_3]^{2+}$ cation in <b>1</b> -(BPh <sub>4</sub> ) <sub>2</sub> showing 30% probability thermal ellipsoids. Hydrogen atoms are omitted for clarity.....	4
Fig. 2 ESI-MS of <b>1</b> in CH <sub>3</sub> CN at room temperature.....	4
Fig. 3 (a) UV-vis spectrum of <b>2</b> in acetonitrile (red) and the reflectance spectrum of a powdered sample of <b>2</b> (black, intensity scale is arbitrary).....	8
Fig. 3 (b) ESI-MS of <b>2</b> in CH <sub>3</sub> CN under N <sub>2</sub> .....	8
Fig. 3 (c) FT-IR spectra of <b>2</b> prepared with BH <sub>4</sub> <sup>-</sup> (red line) and BD <sub>4</sub> <sup>-</sup> (blue line).....	8
Fig. 4 (a) IR spectrum of CH <sub>3</sub> CN (black). (b) IR spectrum of <b>2</b> in CH <sub>3</sub> CN (blue). (c) IR spectrum of a powdered sample of <b>2</b> (red).....	9
Fig. 5 X-ray structure of the $[\text{Ni}(\text{Me}_3\text{-TACN})(\text{BH}_4)(\text{CH}_3\text{CN})]^+$ cation in <b>2</b> -(BPh <sub>4</sub> ) showing 30% probability thermal ellipsoids.....	9
Fig. 6 Reactions of <b>2</b> with chloroform (CHCl <sub>3</sub> ) in CH <sub>3</sub> CN.....	14
Fig. 7 ESI-MS spectrum showing the formation of $[\text{Ni}(\text{Me}_3\text{-TACN})(\text{Cl})]^+$ after the reaction of <b>2</b> and CHCl <sub>3</sub> .....	15
Fig. 8 TD-DFT predicted absorption spectrum of $[\text{Ni}(\text{Me}_3\text{-TACN})(\text{Cl})]^+$ . Inset shows DFT structure of $[\text{Ni}(\text{Me}_3\text{-TACN})(\text{Cl})]^+$ (gray, C; blue, N; green, Ni; gold, Cl).....	16

Fig. 9 Hammett plot of $\log k_2$ against $\sigma_p^+$ of benzoyl chloride derivatives in the reactions of <b>2</b> with <i>para</i> -substituted benzoyl chloride, <i>para</i> -X-Ph-COCl (X = OMe, <sup>t</sup> Bu, H, Cl, NO <sub>2</sub> ) in CH <sub>3</sub> CN at -40 °C.....	18
Fig. 10 (a) DFT structure of <b>2</b> in an $\eta^2$ -fashion (gray, C; blue, N, cyan, H; orange, B; green, Ni). Hydrogen atoms except those attached to boron are omitted for clarity.....	20
Fig. 10 (b) DFT structure of the metastable [Ni(Me <sub>3</sub> -TACN)(BH <sub>4</sub> )] <sup>+</sup> cation in an $\eta^3$ -fashion .....	20

# I . Introduction

## 1.1 Motivation

The nickel–hydrogen interactions are of significant importance in industrial and biological catalytic systems. Nickel–hydrogen complexes are involved in catalytic hydrogenation for organic syntheses,<sup>1–4</sup> nickel hydrogen batteries for rechargeable cells,<sup>5</sup> and hydrogen storage for transportation applications.<sup>6</sup> In nickel-containing enzymes such as hydrogenases, which catalyse the reversible two electron reduction of protons to hydrogen gas, nickel–hydrogen adducts are key intermediates in the proposed mechanisms of the enzymatic reactions.<sup>7–9</sup> One of the eight known nickel enzymes, methyl coenzyme M reductase (MCR), catalyzes the reductive cleavage of the thioether cofactor methyl coenzyme M to produce methane.<sup>10–13</sup>

## 1.2 Previous work

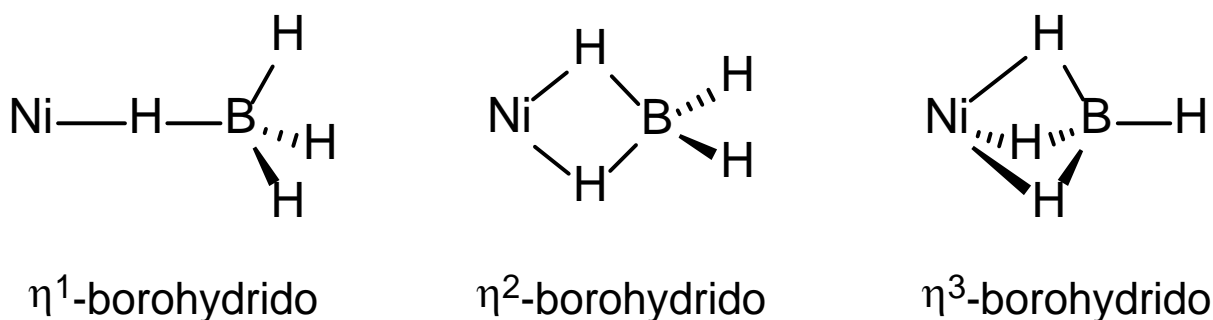
Among the nickel–hydrogen adducts, much attention has recently been focused on nickel–borohydride species, since such adducts are potential materials for nickel-catalyzed hydrogenation.<sup>14</sup> In synthetic chemistry, numerous nickel–borohydride complexes have been prepared and characterized by various spectroscopic and X-ray crystallographic methods, which provided considerable information. The well characterized mononuclear nickel–borohydride species show a variety of hapticities for the borohydride ligand (Scheme 1).<sup>1,15</sup> Cramer and co-workers reported the first example of a single crystal structure of the nickel–borohydride complex bearing a tridentate monoanionic N-donor macrocyclic ligand, [Ni(Tp\*)-(BH<sub>4</sub>)], in an  $\eta^3$ -binding mode, where the importance of ancillary ligands in stabilizing nickel–

borohydride species was emphasized.<sup>16</sup> Its reactivity was also investigated for dehalogenation reactions.

With PCP pincer ligands, Guan et al. described ( $\eta^2$ -BH<sub>4</sub>) nickel(II) complexes by the reaction of the corresponding nickel(II)–hydride complexes and BH<sub>3</sub>.<sup>17</sup> Recently, the reactivity of a similar complex reported by Kirchner and co-workers has been examined in CO<sub>2</sub> reduction.<sup>18</sup> McGrady's group on the other hand reported the ( $\eta^2$ -BH<sub>4</sub>) nickel(I) complex with a tridentate P-donor ligand.<sup>19</sup> Churchard and co-workers were able to isolate two isomers of nickel(II)–borohydride complexes bearing a tetradentate N-donor macrocycle where such complexes were suggested as hydrogen storage materials.<sup>20</sup>

### 1.3 This work

Herein we report the preparation and characterization of a mono-nuclear high-spin ( $\eta^2$ -BH<sub>4</sub>) nickel(II) complex bearing a tridentate N-donor ligand, [Ni(Me<sub>3</sub>-TACN)(BH<sub>4</sub>)(CH<sub>3</sub>CN)]<sup>+</sup> (Me<sub>3</sub>-TACN = 1,4,7-trimethyl-1,4,7-triazacyclononane). To the best of our knowledge, the present study reports not only the first example of a high-spin nickel borohydride complex that has an  $\eta^2$  binding mode but also the first well investigated kinetics in dehalogenation reactions of nickel–borohydride species.



**Scheme 1** Mononuclear nickel-BH<sub>4</sub> adducts with three different coordination modes.

## II. Results and discussion

### 2.1 Nickel(II) precursor complex

The starting complex,  $[\text{Ni}(\text{Me}_3\text{-TACN})(\text{CH}_3\text{CN})_2](\text{ClO}_4)_2$  (**1**- $(\text{ClO}_4)_2$ ), was synthesized by reacting  $\text{Ni}(\text{ClO}_4)_2 \cdot 6\text{H}_2\text{O}$  and  $\text{Me}_3\text{-TACN}$  in  $\text{CH}_3\text{CN}$ . The UV-vis spectrum of **1** in  $\text{CH}_3\text{CN}$  exhibits several d-d bands at 340 ( $\epsilon = 25 \text{ M}^{-1} \text{ cm}^{-1}$ ), 540 ( $\epsilon = 16 \text{ M}^{-1} \text{ cm}^{-1}$ ), 800 ( $\epsilon = 23 \text{ M}^{-1} \text{ cm}^{-1}$ ), and 880 nm ( $\epsilon = 28 \text{ M}^{-1} \text{ cm}^{-1}$ ) (Fig. 1a). The electrospray ionization mass spectrum (ESI-MS) of **1** shows intense isotope envelopes at a mass-to-charge ( $m/z$ ) of 155.6 for  $\{\text{Ni}(\text{Me}_3\text{-TACN})(\text{CH}_3\text{CN})_2\}^{2+}$ , 176.2 for  $\{\text{Ni}(\text{Me}_3\text{-TACN})(\text{CH}_3\text{CN})_3\}^{2+}$  and 369.2 for  $\{\text{Ni}(\text{Me}_3\text{-TACN})(\text{ClO}_4)\}^+$  (Fig. 2). The spin state of **1** in  $\text{CH}_3\text{CN}$  solution was determined using the  $^1\text{H}$  NMR spectroscopy method of Evans, and the room temperature magnetic moment of  $3.2 \mu_{\text{B}}$  indicates a high-spin state ( $S = 1$ ) of the nickel(II) species.<sup>21</sup>

Violet crystals were obtained upon addition of  $\text{NaBPh}_4$  to a solution of **1**- $(\text{ClO}_4)_2$  in  $\text{CH}_3\text{CN}$ . The crystal structure of the cationic part of **1**- $(\text{BPh}_4)_2$  is shown in Fig. 1b and Table 1, and selected bond distances and angles are listed in Table 2. Complex **1** has a distorted octahedral geometry based on facially coordinated  $\text{Me}_3\text{-TACN}$  and three  $\text{CH}_3\text{CN}$  solvent molecules.

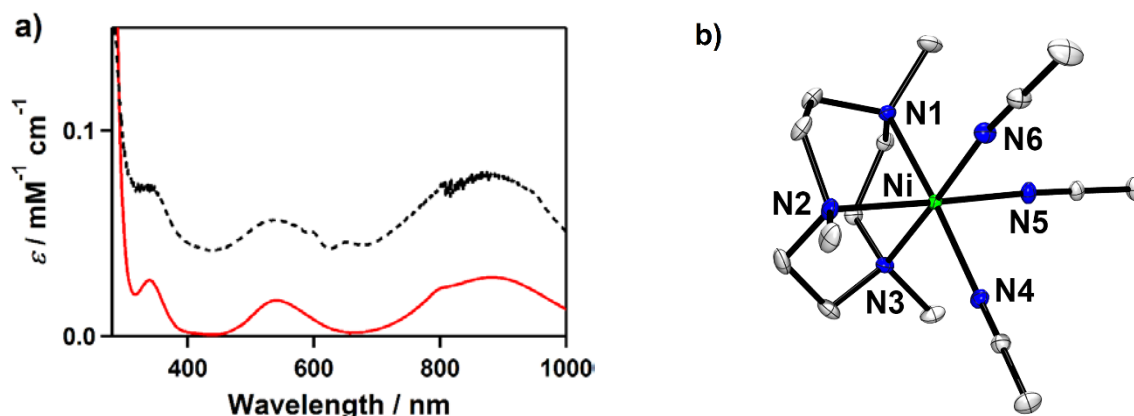


**Fig. 1** (a) UV-vis spectrum of **1** in acetonitrile (red) and the reflectance spectrum of a powdered sample of **1** (black, intensity scale is arbitrary). (b) X-ray structure of the  $[\text{Ni}(\text{Me}_3\text{-TACN})(\text{CH}_3\text{CN})_3]^{2+}$  cation in **1**-(BPh<sub>4</sub>)<sub>2</sub> showing 30% probability thermal ellipsoids. Hydrogen atoms are omitted for clarity.

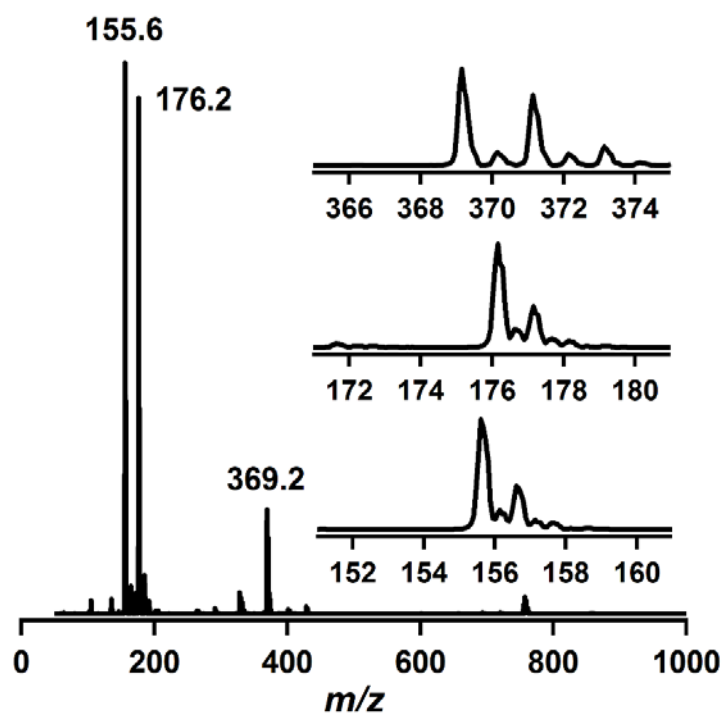
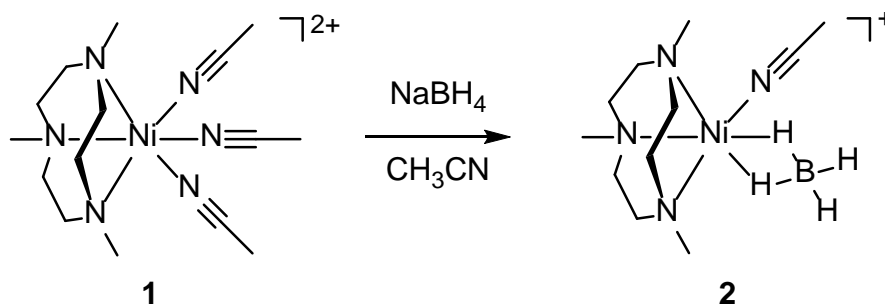


**Fig. 2** ESI-MS of **1** in CH<sub>3</sub>CN at room temperature. Mass peaks at 155.6, 176.2 and 369.2 are assigned to  $[\text{Ni}(\text{Me}_3\text{-TACN})(\text{CH}_3\text{CN})_2]^{2+}$ ,  $[\text{Ni}(\text{Me}_3\text{-TACN})(\text{CH}_3\text{CN})_3]^{2+}$  and  $[\text{Ni}(\text{Me}_3\text{-TACN})(\text{CH}_3\text{CN})(\text{ClO}_4)]^+$ , respectively. Insets show observed distribution patterns for  $[\text{Ni}(\text{Me}_3\text{-TACN})(\text{CH}_3\text{CN})_2]^{2+}$  (bottom),  $[\text{Ni}(\text{Me}_3\text{-TACN})(\text{CH}_3\text{CN})_3]^{2+}$  (middle) and  $[\text{Ni}(\text{Me}_3\text{-TACN})(\text{CH}_3\text{CN})(\text{ClO}_4)]^+$  (upper).

## 2.2 Nickel(II)–borohydride complex and characterization

The nickel(II)–borohydride complex,  $[\text{Ni}(\text{Me}_3\text{-TACN})(\text{BH}_4)(\text{CH}_3\text{CN})]^+$  (**2**), was prepared by adding 1.5 equiv. of  $\text{NaBH}_4$  to a solution containing **1** in  $\text{CH}_3\text{CN}$  at  $-20\text{ }^\circ\text{C}$  under an  $\text{N}_2$  atmosphere, where the color changed from violet to purple (Scheme 2).



**Scheme 2** A synthetic route for a mononuclear nickel(II)-borohydride complex

Complex **2** is thermally stable in  $\text{CH}_3\text{CN}$  under  $\text{N}_2$ , which allowed us to isolate crystals by adding  $\text{NaBH}_4$  that were used in structural and spectroscopic analyses and reactivity studies. The crystalline solid is stable to air and moisture for several days. The UV-vis spectrum of **2** in  $\text{CH}_3\text{CN}$  shows three absorption bands at 355 ( $\epsilon = 23\text{ M}^{-1}\text{ cm}^{-1}$ ), 545 ( $\epsilon = 18\text{ M}^{-1}\text{ cm}^{-1}$ ) and 881 nm ( $\epsilon = 17\text{ M}^{-1}\text{ cm}^{-1}$ ) (Fig. 3a), which are characteristic bands expected for a high-spin  $d^8$  nickel(II) in a distorted octahedral geometry and can be attributed to three possible d–d transitions,  ${}^3\text{A}_{2g} \rightarrow {}^3\text{T}_{1g}(\text{P})$ ,  ${}^3\text{A}_{2g} \rightarrow {}^3\text{T}_{1g}(\text{F})$  and  ${}^3\text{A}_{2g} \rightarrow {}^3\text{T}_{2g}$ , respectively.<sup>22,23</sup> The reflectance spectrum of a powder sample prepared from crystals of **2** shows that the spectral feature of **2** in the solid state is the same as in the solution state (Fig. 3a). The room temperature magnetic moment of  $2.9\ \mu_{\text{B}}$ , determined using the  ${}^1\text{H}$  NMR Evans method, is consistent with a high-spin state ( $S = 1$ ) of the nickel(II) species.<sup>21</sup> The ESI-MS of **2** exhibits a prominent ion peak at a  $m/z$  of 244.2, whose mass and isotope distribution patterns correspond to  $\{\text{Ni}(\text{Me}_3\text{-TACN})(\text{BH}_4)\}^+$  (calculated  $m/z$  of 244.2) (Fig. 3b). When the reaction was carried out with isotopically labeled

NaBD<sub>4</sub>, its mass corresponding to {Ni(Me<sub>3</sub>-TACN)(BD<sub>4</sub>)}<sup>+</sup> appeared at a m/z of 248.2 (calculated m/z of 248.2) (Fig. 3b, inset). The four mass unit shift on substitution of BH<sub>4</sub><sup>-</sup> with BD<sub>4</sub><sup>-</sup> proves that **2** contains a borohydride unit. The Fourier transform infrared (FT-IR) spectrum of **2** shows several isotopically sensitive features (Fig. 3c). [Ni(Me<sub>3</sub>-TACN)(BH<sub>4</sub>)(CH<sub>3</sub>CN)]<sup>+</sup> (**2<sup>H</sup>**) exhibits a strong band at 2428 cm<sup>-1</sup> (doublet, 41 cm<sup>-1</sup> splitting), which shifts to 1809 cm<sup>-1</sup> (doublet, 74 cm<sup>-1</sup> splitting) in [Ni(Me<sub>3</sub>-TACN)(BD<sub>4</sub>)(CH<sub>3</sub>CN)]<sup>+</sup> (**2<sup>D</sup>**). This band has been tentatively assigned to be  $\nu(\text{B-H})_{\text{terminal}}$  and the observed doublet is characteristic of an  $\eta^2$  manner of BH<sub>4</sub><sup>-</sup> binding to the metal center as previously reported.<sup>1,18,20</sup> The observed  $\nu(\text{B-H})/\nu(\text{B-D})$  ratio of 0.75 for  $\nu(\text{B-H})_{\text{terminal}}$  is in good agreement with the calculated ratio of 0.74 based on Hooke's law. According to the literature,<sup>1,20</sup> the bidentate binding of BH<sub>4</sub><sup>-</sup> is of a broad band at 1650 – 2150 for  $\nu(\text{B-H})_{\text{bridging}}$ . In **2<sup>H</sup>**, three isotopically sensitive bands at 2043, 1964 and 1943 cm<sup>-1</sup> are observed in the region of  $\nu(\text{B-H})_{\text{bridging}}$ , which shift to a spectral region obscured by the ligand fingerprint bands in **2<sup>D</sup>**. It was also difficult to observe the lower frequencies for **2** due to the vibrational modes of the supporting ligand. The solution IR spectrum of **2** recorded in CH<sub>3</sub>CN exhibits that the spectral behavior of **2** in solution is the same as that in the solid state (Fig. 4), consistent with the result from UV-vis spectroscopy.

The X-ray crystal structure of [Ni(Me<sub>3</sub>-TACN)(BH<sub>4</sub>)(CH<sub>3</sub>CN)]-(BPh<sub>4</sub>) (**2**-(BPh<sub>4</sub>)) reveals that the borohydride ligand coordinates in a symmetrical  $\eta^2$ -fashion (Fig. 5). The presence of a counter anion, BPh<sub>4</sub><sup>-</sup>, supports the nickel(II) oxidation state assignment. The distorted octahedral nickel center of **2** is bound by three nitrogen atoms of Me<sub>3</sub>-TACN, two bridging hydrogen atoms of BH<sub>4</sub><sup>-</sup>, and one nitrogen atom of CH<sub>3</sub>CN. To the best of our knowledge, this is the first crystal structure of a high-spin nickel(II)-borohydride complex in an  $\eta^2$ -manner.

The Ni...B distance of **2** (2.225(3) Å) is longer than that of the tridentate borohydride

nickel(II) complex,  $[\text{Ni}(\text{Tp}^*)(\eta^2\text{-BH}_4)]$  (2.048 Å);<sup>16</sup> and slightly shorter than that of the bidentate borohydride nickel(I) complex,  $[\text{Ni}(\text{triphos})(\eta^2\text{-BH}_4)]$  (2.24 Å).<sup>19</sup> However, the Ni...B distance of **2** is comparable to that of the bidentate nickel(II) complex,  $[\text{Ni}(\text{PCP}^{\text{Me-iPr}})(\eta^2\text{-BH}_4)]$  (2.218 Å).<sup>18</sup> The average Ni–H bond length of **2** (1.745 Å) is comparable to that of  $[\text{Ni}(\text{PCP}^{\text{Me-iPr}})(\eta^2\text{-BH}_4)]$  (1.78 Å) and lies well within the nickel–borohydride category (1.59–1.94 Å). Based on the structural and spectroscopic characterization, complex **2** is assigned as a high-spin nickel(II)–borohydride complex in an  $\eta^2$ -fashion.

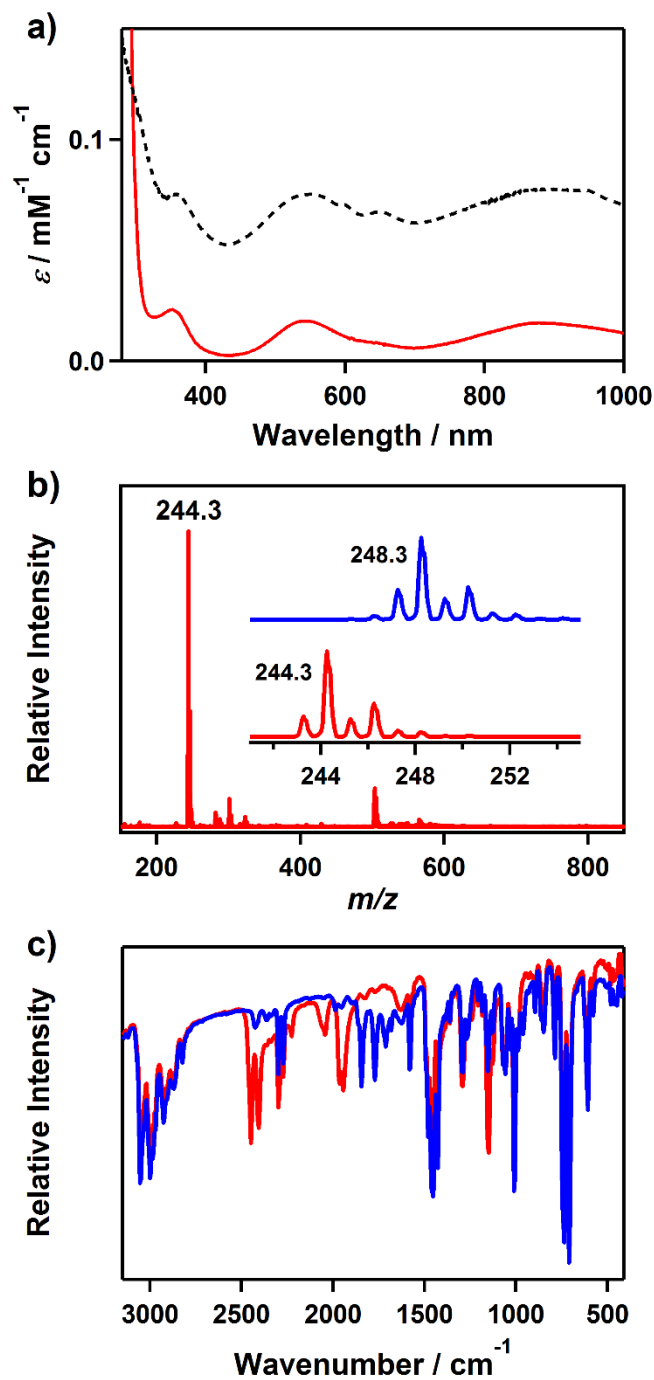


**Fig. 3** (a) UV-vis spectrum of **2** in acetonitrile (red) and the reflectance spectrum of a powdered sample of **2** (black, intensity scale is arbitrary). (b) ESI-MS of **2** in  $\text{CH}_3\text{CN}$  under  $\text{N}_2$ . Inset shows observed isotope distribution patterns for  $\{\text{Ni}(\text{Me}_3\text{-TACN})(\text{BH}_4)\}^+$  at  $m/z$  244.2 (lower) and  $\{\text{Ni}(\text{Me}_3\text{-TACN})(\text{BD}_4)\}^+$  at  $m/z$  248.2 (upper). (c) FT-IR spectra of **2** prepared with  $\text{BH}_4^-$  (red line) and  $\text{BD}_4^-$  (blue line).

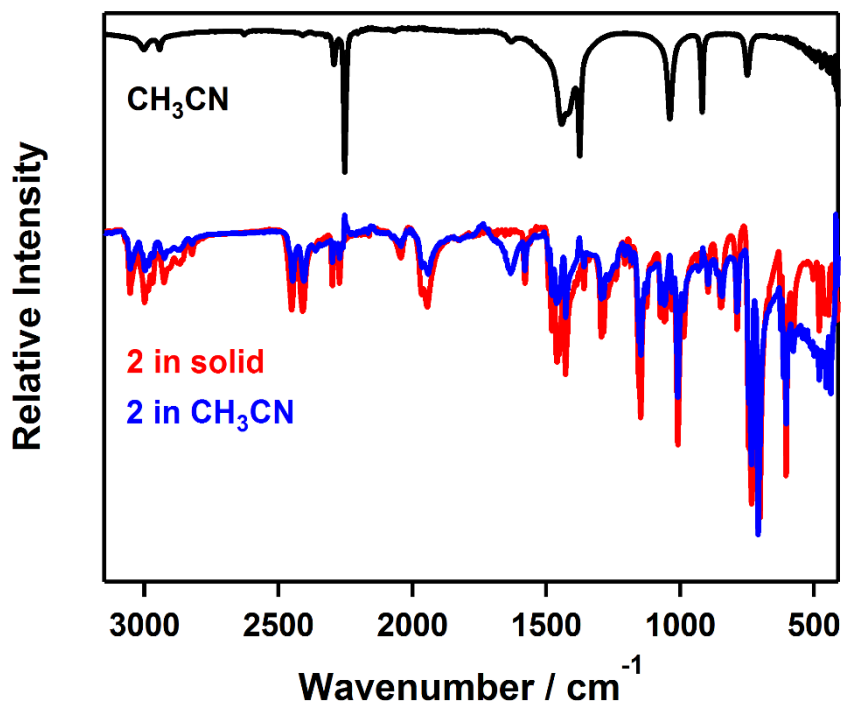


**Fig. 4** (a) IR spectrum of CH<sub>3</sub>CN (black). (b) IR spectrum of 2 in CH<sub>3</sub>CN (blue). (c) IR spectrum of a powdered sample of 2 (red).

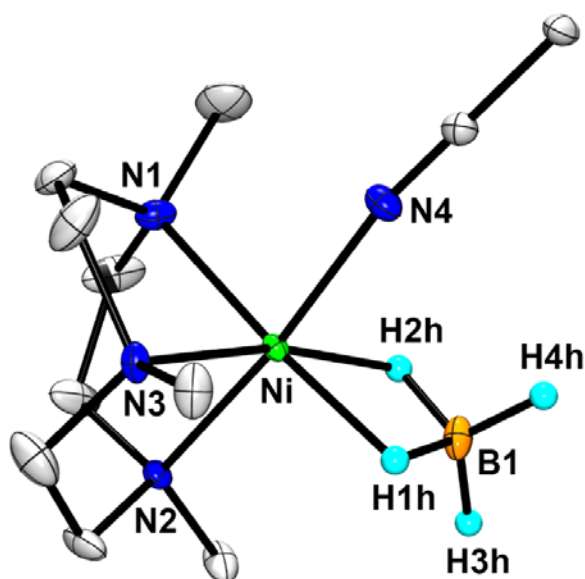


**Fig. 5** X-ray structure of the [Ni(Me<sub>3</sub>-TACN)(BH<sub>4</sub>)(CH<sub>3</sub>CN)]<sup>+</sup> cation in 2-(BPh<sub>4</sub>) showing 30% probability thermal ellipsoids. Hydrogen atoms except those attached to boron are omitted for clarity. Selected bond lengths (Å) and angles (deg): Ni–N1 2.083(2), Ni–N2 2.1430(18), Ni–N3 2.0701(18), Ni–N4 2.0945(19), Ni–H1h 1.72(3), Ni–H2h 1.77(3), Ni···B1 2.225(3), N1–Ni–N2 83.84(7), N2–Ni–N3 84.40(7), N3–Ni–N1 84.92(8).

**Table 1** Crystal data and structure refinements for **1-(BPh<sub>4</sub>)<sub>2</sub>** and **2-(BPh<sub>4</sub>)**

	<b>1-(BPh<sub>4</sub>)<sub>2</sub></b>	<b>2-(BPh<sub>4</sub>)</b>
Empirical formula	C <sub>63</sub> H <sub>70</sub> B <sub>2</sub> N <sub>6</sub> Ni	C <sub>35</sub> H <sub>48</sub> B <sub>2</sub> N <sub>4</sub> Ni
Formula weight	991.58	605.10
Temperature (K)	100(2)	100(2)
Crystal system	Monoclinic	Orthorhombic
space group	<i>P2<sub>1</sub>/c</i>	<i>Pbca</i>
Unit cell dimensions		
<i>a</i> (Å)	18.0900(2)	20.1159(6)
<i>b</i> (Å)	11.65560(10)	15.8862(5)
<i>c</i> (Å)	25.8637(3)	20.4047(6)
β (°)	90.1750(10)	90
Volume (Å <sup>3</sup> )	5453.33(10)	6520.6(3)
<i>Z</i>	4	8
<i>d</i> <sub>calc</sub> (g/cm <sup>-3</sup> )	1.208	1.233
μ (mm <sup>-1</sup> )	0.401	0.625
Reflections collected	95457	110259
Independent reflections	13591	8116
Refinement method	Full-matrix least-squares on <i>F</i> <sup>2</sup>	Full-matrix least-squares on <i>F</i> <sup>2</sup>
<i>F</i> (000)	2112	2592
Goodness-of-fit on <i>F</i> <sup>2</sup>	1.030	1.070
Final <i>R</i> indices [ <i>I</i> > 2σ( <i>I</i> )]	<i>R</i> <sub>1</sub> = 0.0303, <i>wR</i> <sub>2</sub> = 0.0775	<i>R</i> <sub>1</sub> = 0.0524, <i>wR</i> <sub>2</sub> = 0.1251
<i>R</i> indices (all data)	<i>R</i> <sub>1</sub> = 0.0361, <i>wR</i> <sub>2</sub> = 0.0775	<i>R</i> <sub>1</sub> = 0.0573, <i>wR</i> <sub>2</sub> = 0.1291

**Table 2.** Selected bond distances (Å) and angles (°) for **1**-(BPh<sub>4</sub>)<sub>2</sub> and **2**-BPh<sub>4</sub>.

Bond Distances (Å)			
<b>1</b> -(BPh <sub>4</sub> ) <sub>2</sub>		<b>2</b> -BPh <sub>4</sub>	
Ni1-N1	2.1034(10)	Ni1-N1	2.083(2)
Ni1-N2	2.1019(10)	Ni1-N2	2.1430(18)
Ni1-N3	2.0998(10)	Ni1-N3	2.0701(18)
Ni1-N4	2.1169(10)	Ni1-N4	2.0945(19)
Ni1-N5	2.0619(10)	Ni1-H1h	1.72(3)
Ni1-N6	2.0869(10)	Ni1-H2h	1.77(3)
		Ni1···B1	2.225(3)

Bond Angles (°)			
<b>1</b> -(BPh <sub>4</sub> ) <sub>2</sub>		<b>2</b> -BPh <sub>4</sub>	
N1-Ni1-N2	84.50(4)	N1-Ni1-N2	83.84(7)
N1-Ni1-N3	84.46(4)	N1-Ni1-N3	84.92(8)
N1-Ni1-N4	176.61(4)	N1-Ni1-N4	91.71(8)
N1-Ni1-N5	92.30(4)	N2-Ni1-N3	84.40(7)
N1-Ni1-N6	94.75(4)	N2-Ni1-N4	174.60(8)
N2-Ni1-N3	84.55(4)	N3-Ni1-N4	92.18(8)
N2-Ni1-N4	92.16(4)		
Ni2-Ni1-N5	176.17(4)		
Ni2-Ni1-N6	93.19(4)		

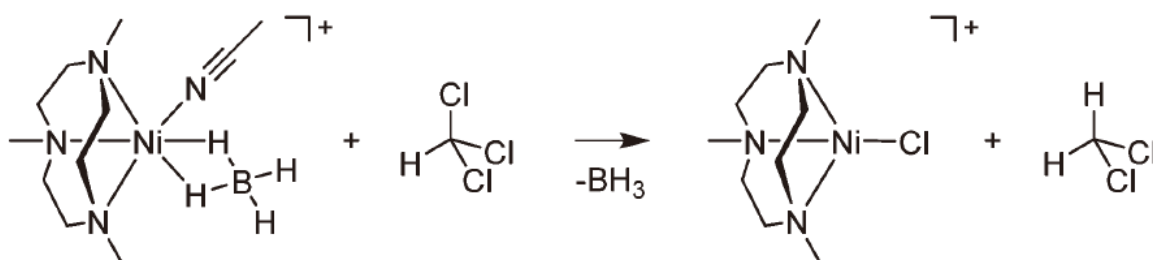
### 2.3 Reactivity

It is known that mononuclear metal–borohydride complexes are capable of performing reductive dehalogenation of halocarbons.<sup>16,19,24,25</sup> In order to examine the dehalogenation reactivity of **2**, we carried out the reaction of CHCl<sub>3</sub> with **2**. Upon the addition of CHCl<sub>3</sub> to **2** in CH<sub>3</sub>CN at 25 °C, the UV-vis absorption bands of **2** disappeared with a pseudo-first-order decay (Fig. 6a, inset). Product analysis of the final reaction mixture revealed the formation of CH<sub>2</sub>Cl<sub>2</sub> and very little H<sub>2</sub>, where the volatile products were confirmed by <sup>1</sup>H NMR.<sup>16,26</sup> In addition, [Ni(Me<sub>3</sub>-TACN)(Cl)]<sup>+</sup> was found in the reaction solutions as a product of **2** (Fig. 7 for ESI-MS analysis). Although several attempts to isolate the product as crystals have not been successful, an intense band at 342 nm of the product solution is similar to that of previously reported tetrahedral Ni(II)–Cl complexes (Fig. 6a).<sup>27</sup> These bands have been assigned to the Cl pπ → Ni dπ\* LMCT band on the basis of theoretical calculations (Fig. 8).<sup>28</sup>

The pseudo-first-order rate constants, monitored at 545 nm, increased proportionally with the CHCl<sub>3</sub> concentration, giving a second-order rate constant (*k*<sub>2</sub>) of 2.7(1) × 10<sup>-3</sup> M<sup>-1</sup> s<sup>-1</sup> (Fig. 6b). The rates were dependent on the reaction temperature, where a linear Eyring plot was observed in the range of 278 – 308 K with activation parameters of Δ*H*<sup>‡</sup> = 33 kJ mol<sup>-1</sup> and Δ*S*<sup>‡</sup> = -182 J mol<sup>-1</sup> K<sup>-1</sup> (Fig. 6c). The observed negative entropy value and second-order kinetics suggest that a bimolecular mechanism is performing in the reduction of CHCl<sub>3</sub> by **2** (Scheme 3). The reactivity of **2** in dehalogenation is much higher than that of the low-spin (η<sup>3</sup>-BH<sub>4</sub>) nickel(II) complex, [Ni(Tp\*)(BH<sub>4</sub>)], where the latter reacted with CHCl<sub>3</sub> only at elevated temperatures (>50 °C).<sup>16,18</sup>

We also observed a kinetic isotope effect (KIE) value of 1.7 in the reduction of CHCl<sub>3</sub> by

**2** when **2<sup>H</sup>** was replaced with **2<sup>D</sup>** (Fig. 6b). This KIE value is comparable to that of [Ni(Tp\*)-(BH<sub>4</sub>)] ( $k_H/k_D = 3$ ),<sup>16</sup> in which hydride ion or hydrogen atom transfer was proposed to be rate limiting.



**Scheme 3** Proposed mechanism of the dehalogenation of CHCl<sub>3</sub> by **2**.

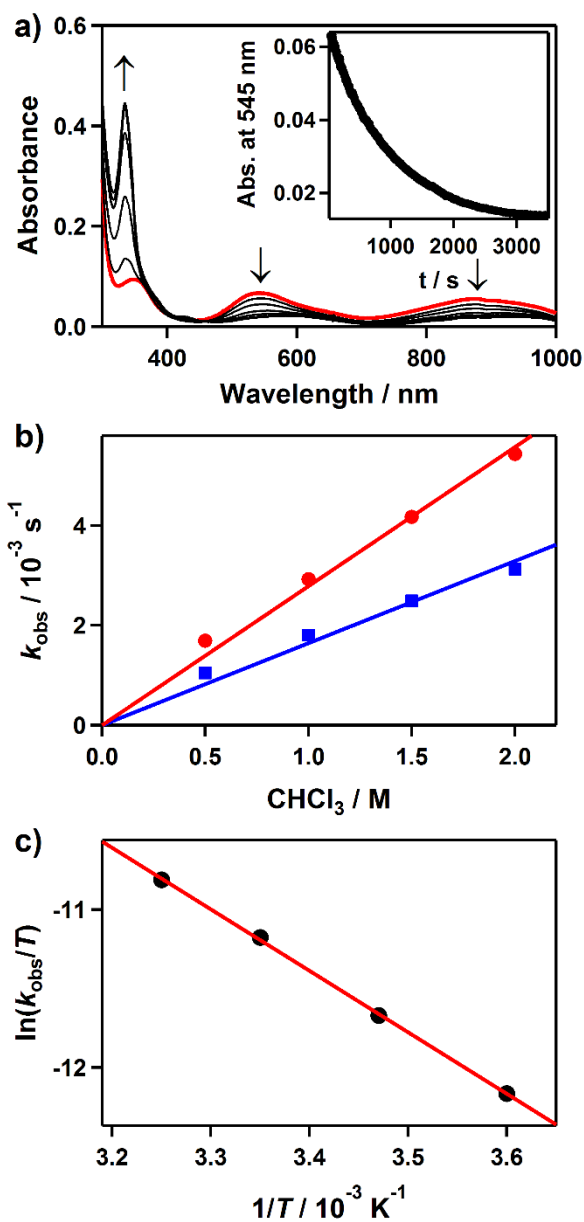


**Fig. 6** Reactions of **2** with chloroform ( $\text{CHCl}_3$ ) in  $\text{CH}_3\text{CN}$ . (a) UV-vis spectral changes of **2** (4 mM) upon addition of 125 equiv. of  $\text{CHCl}_3$  at 25 °C. Inset shows the time course of the absorbance at 545 nm. (b) Plots of  $k_{\text{obs}}$  against the concentration of  $\text{CHCl}_3$  to determine second-order rate constants for the reactions of **2**<sup>H</sup> (red line with  $\bullet$ ) and **2**<sup>D</sup> (blue line with  $\blacksquare$ ) at 25 °C. (c) Plot of second-order rate constants against  $1/T$  to determine activation parameters for the reaction of **2** and  $\text{CHCl}_3$ .

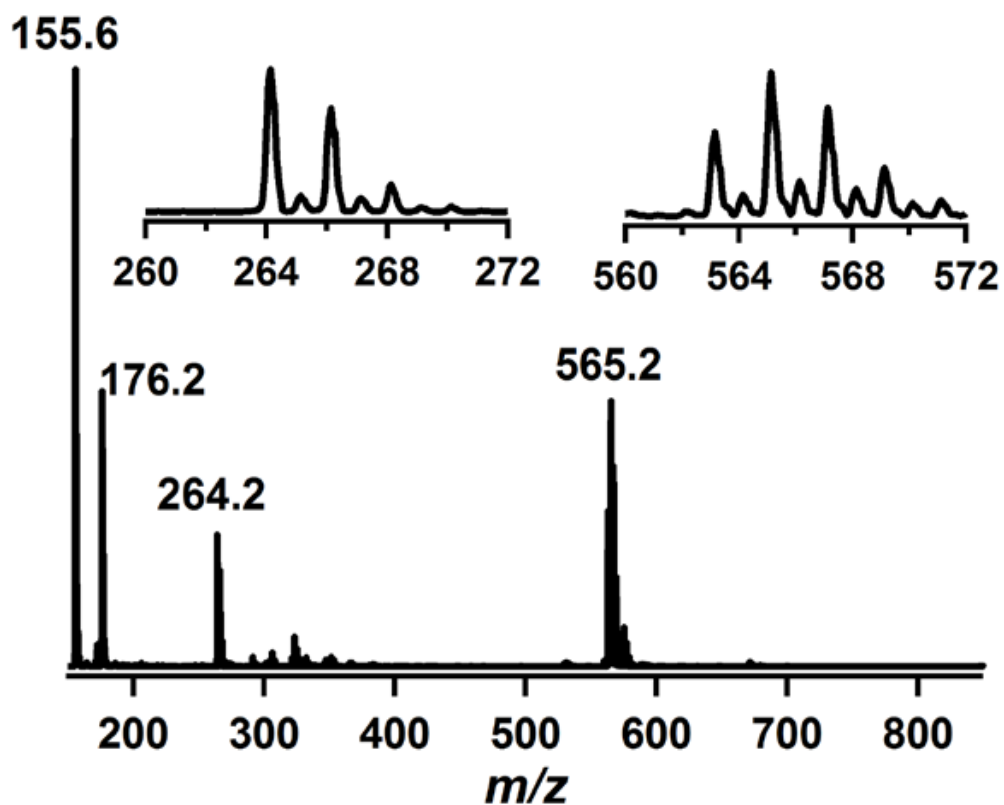


**Fig. 7** ESI-MS spectrum showing the formation of  $[Ni(Me_3-TACN)(Cl)]^+$  after the reaction of **2** and  $CHCl_3$ . Mass peaks at 155.6, 176.2, 264.2 and 565.2 are assigned to  $[Ni(Me_3-TACN)(CH_3CN)_2]^{2+}$ ,  $[Ni(Me_3-TACN)(CH_3CN)_3]^{2+}$ ,  $[Ni(Me_3-TACN)(Cl)]^+$  and  $[Ni_2(Me_3-TACN)_2(Cl)_3]^+$ , respectively. Insets show observed distribution patterns for  $[Ni(Me_3-TACN)(Cl)]^+$  (left) and  $[Ni_2(Me_3-TACN)_2(Cl)_3]^+$  (right).

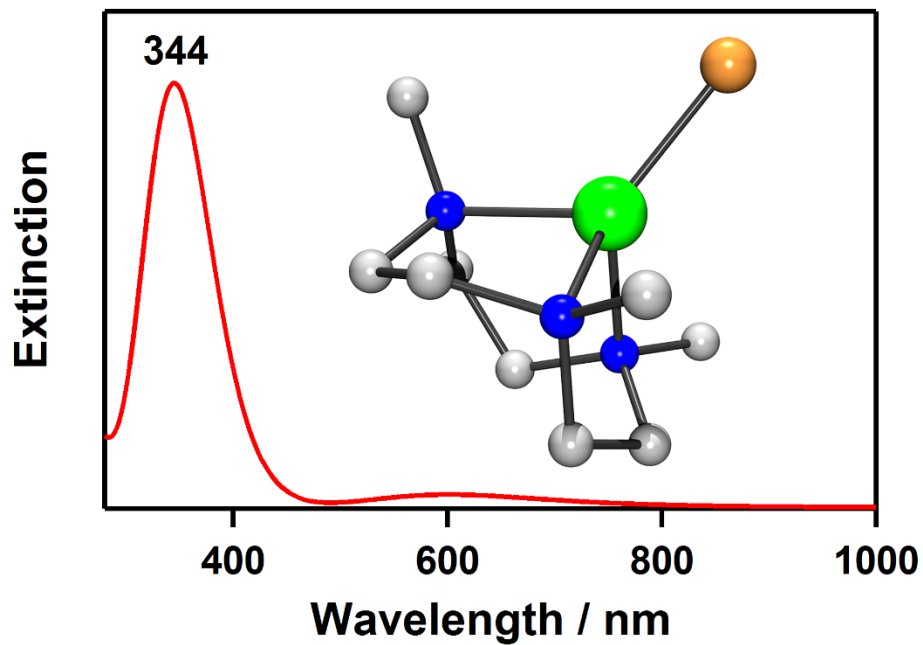


**Fig. 8** TD-DFT predicted absorption spectrum of [Ni(Me<sub>3</sub>-TACN)(Cl)]<sup>+</sup>. Inset shows DFT structure of [Ni(Me<sub>3</sub>-TACN)(Cl)]<sup>+</sup> (gray, C; blue, N; green, Ni; gold, Cl).

The reactivity of **2** was further investigated using *para*-substituted benzoyl chloride, which has a series of electron-donating and -withdrawing substituents at the *para*-position of the phenyl group (*para*-X-Ph-COCl; X = MeO, <sup>t</sup>Bu, H, Cl, NO<sub>2</sub>). **2** disappeared immediately upon addition of benzoyl chloride (10 equiv.) in CH<sub>3</sub>CN at -40 °C. Thus, the reactivity of **2** with *para*-substituted benzoyl chloride was examined using a stopped-flow spectrometer. The Hammett plot of the second-order rate constants vs.  $\sigma_p^+$  gave a  $\rho$  value of 1.2 (Fig. 9). The positive  $\rho$  value is consistent with the process involving a nucleophilic character. Product analysis of the final reaction mixture revealed the formation of *para*-substituted benzaldehydes.

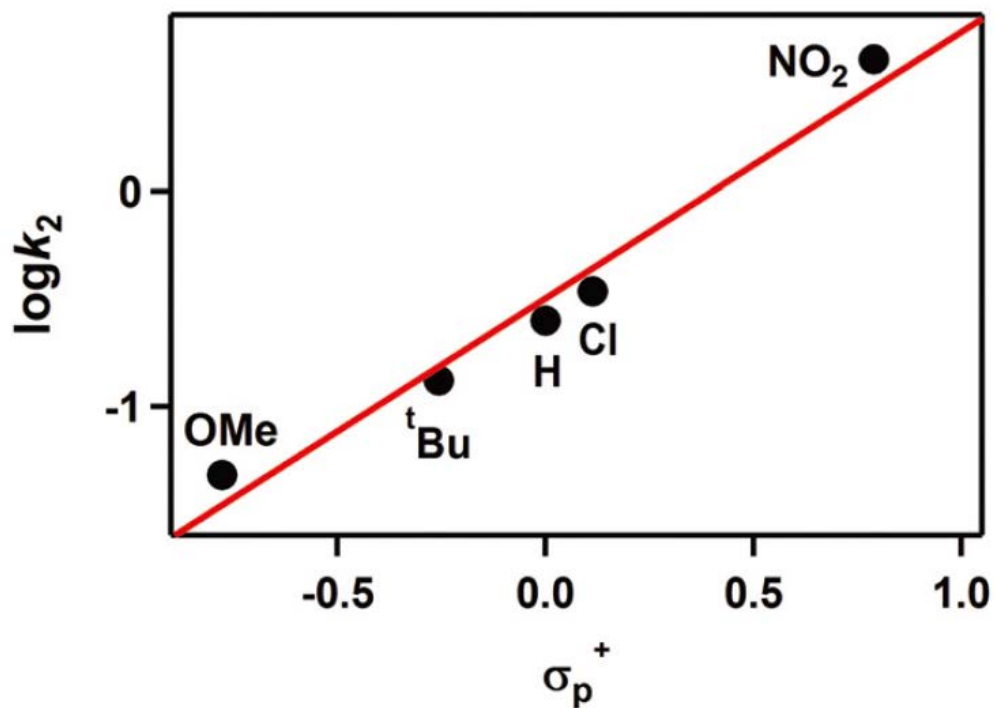


**Fig. 9** Hammett plot of  $\log k_2$  against  $\sigma_p^+$  of benzoyl chloride derivatives in the reactions of **2** with *para*-substituted benzoyl chloride, *para*-X-Ph-COCl (X = OMe, <sup>t</sup>Bu, H, Cl, NO<sub>2</sub>) in CH<sub>3</sub>CN at -40 °C.

## 2.4 Density functional theory results

To compare the stability of the Ni(II)–borohydride complexes in different coordination modes at a quantitative level, we performed spin-polarized density functional theory (DFT) calculations of the complexes in the gas phase using a non-local hybrid exchange–correlation functional (B3LYP).<sup>29</sup> Two different coordination modes,  $\eta^2$  and  $\eta^3$ , were considered (Fig. 10). Both complexes are in a high-spin state ( $S = 1$ ). For the  $[\text{Ni}(\text{Me}_3\text{-TACN})(\text{BH}_4)(\text{CH}_3\text{CN})]^+$  cation in an  $\eta^2$ -fashion, the Ni $\cdots$ B distance is calculated to be 2.19 Å and the average Ni–H bond length is 1.75 Å, in good agreement with the experimental values. For the  $[\text{Ni}(\text{Me}_3\text{-TACN})(\text{BH}_4)]^+$  cation in an  $\eta^3$ -fashion, the Ni $\cdots$ B distance is shortened to 1.97 Å, while the Ni–H bonds are elongated with the average value of 1.85 Å. We found that the  $\eta^2$ -complex is 35 kJ mol<sup>-1</sup> more stable than the  $\eta^3$ -complex, indicating that the Ni(II)–borohydride will exist in an  $\eta^2$ -fashion in a solution at room temperature.

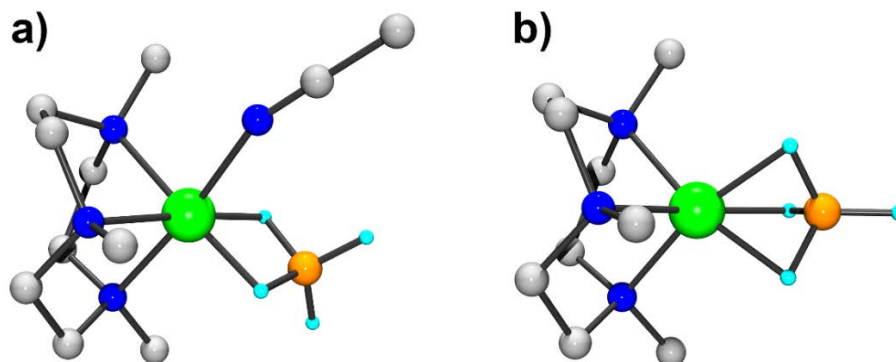


**Fig. 10** (a) DFT structure of **2** in an  $\eta^2$ -fashion (gray, C; blue, N, cyan, H; orange, B; green, Ni). Hydrogen atoms except those attached to boron are omitted for clarity. Selected bond lengths ( $\text{\AA}$ ) and angles (deg) are listed below for a direct comparison with the result in Fig. 3: Ni–N1 2.14, Ni–N2 2.20, Ni–N3 2.15, Ni–N4 2.17, Ni–H1h 1.76, Ni–H2h 1.75, Ni $\cdots$ B1 2.19, N1–Ni–N2 83.26, N2–Ni–N3 82.95, N3–Ni–N1 83.85. (b) DFT structure of the metastable  $[\text{Ni}(\text{Me}_3\text{-TACN})(\text{BH}_4)]^+$  cation in an  $\eta^3$ -fashion.

**Table 3.** Coordinates in xyz-format

---

[Ni(Me <sub>3</sub> -TACN)(BH <sub>4</sub> )(CH <sub>3</sub> CN)] <sup>+</sup>			
C	0.540141990789	-1.910107262329	-3.339115379300
C	2.598635500717	-1.215857630127	-2.271431301980
C	-0.870075162044	-1.520954368623	-3.760113434469
C	1.578786011763	0.259925035689	-3.920281918564
C	-2.527329408721	-1.523360240791	-1.973383907107
C	1.253121585663	1.672907839219	-3.455214746106
C	-2.214208355842	0.501162661760	-3.301166064797
C	-1.193714309899	1.511244250221	-3.825170941530
C	-0.258417909946	3.092451665042	-2.205437313636
C	-2.206842997904	1.423529222414	0.727943471123
C	-2.913588099744	1.851000180526	1.917392105009
H	3.205635267900	-1.720377687148	-3.031228884446
H	1.044823080704	-2.406418889837	-4.177430103760
H	0.497944410581	-2.625787231692	-2.517302832770
H	2.400709199324	-1.898484473105	-1.450321143179

H	-1.444436307466	-2.428235500753	-3.957311708826
H	3.151988217855	-0.368913125300	-1.873592313032
H	2.626528588432	0.225446774025	-4.224825824757
H	-0.851517162677	-0.969572122090	-4.698264562861
H	1.002282534207	0.006556027999	-4.808307383334
H	1.997943109191	-0.858443523761	0.561596704916
H	-2.008872972450	-2.363996245178	-1.515837782629
H	-3.312594114889	-1.905281182294	-2.633694479479
H	0.139792599204	-1.063318462701	-0.178218127886
H	1.124493428981	0.733668878815	-0.289208769952
H	-2.903415297491	0.224744977343	-4.107470094000
H	-2.981649184290	-0.931043413969	-1.183522061972
H	-0.760414289878	1.162661006421	-4.760527468198
H	1.966917946085	1.980303870221	-2.690148159647
H	0.429277482494	0.054995946950	1.475545880128
H	1.352315278251	2.370728515664	-4.295383797790
H	-2.806361259142	0.952768267464	-2.507240646068

H	-1.709259406785	2.443495053188	-4.062837932938
H	0.484893951837	3.211803891073	-1.419079223959
H	-0.138778513489	3.897715747444	-2.937557429219
H	-1.246740424017	3.164827505470	-1.759802533736
H	-2.663500650948	1.184386065824	2.743559915322
H	-2.619115467966	2.867740603075	2.178380272448
H	-3.989566741025	1.822893122252	1.743221165290
B	0.950388772884	-0.296294272819	0.458608608331
N	1.321223203556	-0.749233046637	-2.853549794293
N	-1.556711336720	-0.696485346854	-2.722572670573
N	-0.096068481454	1.767518513081	-2.843073972243
N	-1.636268123659	1.073758752954	-0.206755145065
Ni	-0.082138453419	0.163115139869	-1.420693796011

---

---

---

[Ni(Me<sub>3</sub>-TACN)(BH<sub>4</sub>)<sup>+</sup>

---

C	0.614133357328	-1.906288728906	-3.551474049915
C	2.780351495561	-1.324878900944	-2.584407875827
C	-0.833578038916	-1.453367118763	-3.726327989218
C	1.650279535469	0.300570836305	-4.030908830348
C	-2.199273737041	-1.591572068709	-1.692221778771
C	1.423704434195	1.667569758124	-3.387573570649
C	-2.024673474164	0.544852841382	-2.860633883962
C	-1.055959564112	1.576094509827	-3.432021298395
C	0.114378036743	2.899492187053	-1.732495290403
C	-5.408794077906	2.407040344746	5.945918748203
C	-6.290065261234	2.540016475912	7.095236272421
H	3.325402128075	-1.795674010349	-3.407728774767
H	0.997948331399	-2.304533050589	-4.497559583741
H	0.665646702389	-2.710210804104	-2.816653616008
H	2.626472212284	-2.053024964331	-1.791106165299
H	-1.460668537664	-2.324519259840	-3.924637733116
H	3.375406523246	-0.506694806361	-2.183358123596
H	2.654512714420	0.263724562933	-4.458076086592
H	-0.929307970532	-0.808589105752	-4.597558601977
H	0.965208990342	0.150613545066	-4.862975206222
H	0.952197789162	-0.336487804856	1.633052482890

H	-1.660610691554	-2.499384940818	-1.428206984749
H	-3.111577007644	-1.861066373800	-2.232396556933
H	0.599655012244	-1.335481922387	-0.124266331184
H	1.612759576097	0.388773394329	-0.168366766815
H	-2.844164451349	0.371070709752	-3.567025908772
H	-2.464802664753	-1.072453474895	-0.773504154389
H	-0.768584306652	1.311026449810	-4.447448301706
H	2.239659003034	1.895127946586	-2.700940793217
H	-0.347332603075	0.390520810319	0.221572945042
H	1.419012483993	2.445703546535	-4.159408723608
H	-2.466579634544	0.922245943550	-1.937749403735
H	-1.557038982054	2.543505553570	-3.502699824526
H	0.962130472939	2.905817452960	-1.051041727147
H	0.126739135802	3.810452498433	-2.338193919451
H	-0.798951438884	2.880329417921	-1.140479108472
H	-7.106787365241	3.224646449295	6.863131140973
H	-6.704850262789	1.566419355500	7.359761864000
H	-5.739032191482	2.928642215962	7.951873929135
B	0.720909055161	-0.230823952062	0.480637409174
N	1.472588467813	-0.805387120559	-3.043151242266
N	-1.330182468640	-0.724187177282	-2.520445430696
N	0.172858847304	1.692961438592	-2.589358992767
N	-4.713307297959	2.300920557031	5.033179421853

Ni	0.342357618856	-0.059403461935	-1.441497975135
----	----------------	-----------------	-----------------

---

---

## III. Conclusions

### 3.1 Conclusions

A mononuclear high-spin ( $\eta^2$ -BH<sub>4</sub>) nickel(II) complex, [Ni(Me<sub>3</sub>-TACN)(BH<sub>4</sub>)(CH<sub>3</sub>CN)]<sup>+</sup> (**2**), has been successfully prepared and characterized by various physicochemical methods. In particular, FT-IR spectroscopy together with X-ray crystallography clearly shows that a borohydride is bound to the nickel center in an  $\eta^2$ -fashion. **2** is capable of performing dehalogenation reactions. Kinetic studies and isotope labelling experiments suggest that bimolecular collision between **2** and halocarbons is the rate-limiting step in dehalogenation reactions.

## IV. Experimental section

### 4.1 Materials

All chemicals obtained from Aldrich Chemical Co. were of the best available purity and used without further purification unless otherwise indicated. Solvents were dried according to published procedures and distilled under Ar prior to use.<sup>30</sup>

### 4.2 Physical methods

UV-vis spectra were recorded on a Hewlett Packard 8453 diode array spectrophotometer equipped with UNISOKU Scientific Instruments for low-temperature experiments or with a circulating water bath. Fast reactions were monitored using a Hi-Tech Scientific SF-61 DX2 cryogenic stopped-flow spectrometer equipped with a Xe arc lamp and a KinetaScan diode array rapid scanning unit. Electrospray ionization mass spectra (ESI-MS) were collected on a Waters (Milford, MA, USA) Acquity SQD quadrupole mass instrument, by infusing samples directly into the source using a manual method. The spray voltage was set at 2.5 kV and the capillary temperature at 80 °C. Infrared spectra were recorded on a Thermo Scientific Nicolet iS10 FT-IR spectrometer equipped with a diamond attenuated total reflectance (ATR) accessory. The effective magnetic moments were determined using the modified <sup>1</sup>H NMR method of Evans at room temperature.<sup>21,31,32</sup> A WILMAD® coaxial insert (sealed capillary) tube containing the blank acetonitrile-*d*<sub>3</sub> solvent (with 1.0% TMS) only was inserted into the normal NMR tubes containing the complexes dissolved in acetonitrile-*d*<sub>3</sub> (with 0.03% TMS). The chemical shift of the TMS peak (and / or the solvent peak) in the presence of the paramagnetic metal complexes was compared with that of the TMS peak (and / or the solvent peak) in the

inner coaxial insert tube. The effective magnetic moment was calculated using the equation,  $\mu = 0.0618(\Delta\nu T/2fM)^{1/2}$ , where  $f$  is the oscillator frequency (MHz) of the superconducting spectrometer,  $T$  is the absolute temperature,  $M$  is the molar concentration of the metal ion, and  $\Delta\nu$  is the difference in frequency (Hz) between the two reference signals. Product analysis was performed on a Thermo Fisher Trace 1310 gas chromatograph system equipped with a flame ionization detector (GC).  $^1\text{H}$  NMR spectra were recorded with a Bruker AVANCE III-400 spectrometer at CCRF in DGIST.

### 4.3 Syntheses

#### 4.3.1 $[\text{Ni}(\text{Me}_3\text{-TACN})(\text{CH}_3\text{CN})_2](\text{ClO}_4)_2$ (**1**- $(\text{ClO}_4)_2$ ).

$\text{Me}_3\text{-TACN}$  (0.1 g, 0.58 mmol) was added to an acetonitrile solution (30 mL) of  $\text{Ni}(\text{ClO}_4)_2 \cdot 6\text{H}_2\text{O}$  (0.212 g, 0.58 mmol) and tetra-methylethylenediamine (0.067 g, 0.58 mmol). The resulting solution was refluxed for 12 h, affording a pink solution. After cooling to room temperature, the solvent was removed under reduced pressure to give a pink powder. The solid was filtered and the filtrate was then washed with diethyl ether and dried in a vacuum. Yield: 0.29 g (90%). ESI-MS (in  $\text{CH}_3\text{CN}$ ):  $m/z$  155.6 for  $\{\text{Ni}(\text{Me}_3\text{-TACN})(\text{CH}_3\text{CN})_2\}^{2+}$  and 176.2 for  $\{\text{Ni}(\text{Me}_3\text{-TACN})(\text{CH}_3\text{CN})_3\}^{2+}$ . Anal. Calcd for  $\text{C}_{13}\text{H}_{27}\text{Cl}_2\text{N}_5\text{NiO}_8$ : C, 30.56; H, 5.33; N, 13.71. Found: C, 30.58; H, 5.49; N, 13.99. X-ray crystallographically suitable crystals were obtained by addition of  $\text{NaBPh}_4$ .

#### 4.3.2 $[\text{Ni}(\text{Me}_3\text{-TACN})(\text{BH}_4)(\text{CH}_3\text{CN})](\text{BPh}_4)$ (**2**- $(\text{BPh}_4)$ ).

Treatment of **1** (0.051 g, 0.1 mmol) in  $\text{CH}_3\text{CN}$  (1 mL) with 1.5 equiv. of  $\text{NaBH}_4$  (0.006 g, 0.15 mmol) at  $-20\text{ }^\circ\text{C}$  under  $\text{N}_2$  afforded the formation of a purple solution, to which was

added NaBPh<sub>4</sub> (0.034 g, 0.1 mmol). The resulting solution was allowed to stand for several days at -20 °C, giving dark purple crystals suitable for X-ray crystallography. Crystalline yield: 0.043 g (71%). ESI-MS (in CH<sub>3</sub>CN): m/z 244.2 for {Ni(Me<sub>3</sub>-TACN)(BH<sub>4</sub>)}<sup>+</sup>. Anal. Calcd for C<sub>35</sub>H<sub>48</sub>B<sub>2</sub>N<sub>4</sub>Ni: C, 69.47; H, 8.00; N, 9.26. Found: C, 69.12; H, 7.71; N, 9.55.

#### 4.4 X-ray crystallography

Single crystals of [Ni(Me<sub>3</sub>-TACN)(CH<sub>3</sub>CN)<sub>3</sub>](BPh<sub>4</sub>)<sub>2</sub> (**1**-(BPh<sub>4</sub>)<sub>2</sub>) and [Ni(Me<sub>3</sub>-TACN)(BH<sub>4</sub>)(CH<sub>3</sub>CN)](BPh<sub>4</sub>) (**2**-(BPh<sub>4</sub>)) were picked from solutions by using a nylon loop (Hampton Research Co.) on a handmade copper plate mounted inside a liquid N<sub>2</sub> Dewar vessel at *ca.* -40 °C and mounted on a goniometer head in a N<sub>2</sub> cryostream. Data collections were carried out on a Bruker SMART APEX II CCD diffractometer equipped with a monochromator in the Mo K $\alpha$  ( $\lambda = 0.71073$  Å) incident beam. The CCD data were integrated and scaled using the Bruker-S SAINT software package, and the structure was solved and refined using SHELXTL V 6.12.<sup>33</sup> Hydrogen atoms were located in the calculated positions except those of borohydride, which were found from the Fourier difference map. All non-hydrogen atoms were refined with anisotropic thermal parameters. Crystal data for **1**-(BPh<sub>4</sub>)<sub>2</sub>: C<sub>63</sub>H<sub>70</sub>B<sub>2</sub>N<sub>6</sub>Ni, monoclinic, *P*2<sub>1</sub>/*c*, *Z* = 4,  $\alpha = 18.0900(2)$ ,  $b = 11.65560(10)$ ,  $c = 25.8637(3)$  Å,  $\beta = 90.1750(10)^\circ$ ,  $V = 5453.33(10)$  Å<sup>3</sup>,  $\mu = 0.401$  mm<sup>-1</sup>,  $\rho_{\text{calcd}} = 1.208$  g cm<sup>-3</sup>,  $R_1 = 0.0303$ ,  $wR_2 = 0.0775$  for 13591 unique reflections, 655 variables. Crystal data for **2**-(BPh<sub>4</sub>): C<sub>35</sub>H<sub>48</sub>B<sub>2</sub>N<sub>4</sub>Ni, orthorhombic, *Pbca*, *Z* = 8,  $\alpha = 20.1159(6)$ ,  $b = 15.8862(5)$ ,  $c = 20.4047(6)$  Å,  $V = 6520.6(3)$  Å<sup>3</sup>,  $\mu = 0.625$  mm<sup>-1</sup>,  $\rho_{\text{calcd}} = 1.233$  g cm<sup>-3</sup>,  $R_1 = 0.0524$ ,  $wR_2 = 0.1251$  for 8116 unique reflections, 399 variables. The crystallographic data for **1**-(BPh<sub>4</sub>)<sub>2</sub> and **2**-(BPh<sub>4</sub>) are listed in Table 1, and Table 2 lists the selected bond distances and angles.

#### 4.5 Reactivity

All reactions were run in a 1 cm UV cuvette by monitoring UV-vis spectral changes of reaction solutions, and rate constants were determined by fitting the changes in absorbance at 545 nm for  $[\text{Ni}(\text{Me}_3\text{-TACN})(\text{BH}_4)(\text{CH}_3\text{CN})]^+$  (**2**). For the stopped-flow experiments, all reaction traces were collected at  $-40\text{ }^\circ\text{C}$ . The raw kinetic data were treated with KinetAsyst 3 (Hi-Tech Scientific) and Specfit/32 Global Analysis System software from Spectrum Software Associates. Reactions were run at least in triplicate, and the data reported represent the average of these reactions. Crystalline samples of **2** were used in kinetic studies, such as the reduction of chloroform in  $\text{CH}_3\text{CN}$  at  $25\text{ }^\circ\text{C}$ . After the completion of reactions, pseudo-first-order fitting of the kinetic data allowed us to determine  $k_{\text{obs}}$  values. Products formed in the reduction of chloroform by **2** in  $\text{CD}_3\text{CN}$  at  $25\text{ }^\circ\text{C}$  were analyzed by  $^1\text{H}$  NMR. Products were identified by comparing with authentic samples.

#### 4.6 Computational details

Spin-polarized DFT calculations were performed using a non-local hybrid exchange–correlation functional (B3LYP).<sup>29</sup> We used the projector-augmented wave (PAW) method<sup>34</sup> and a plane wave cutoff of 400 eV, as implemented in the VASP code.<sup>35,36</sup> Atomic structures of the Ni(II)–borohydride complexes were relaxed within  $0.03\text{ eV } \text{\AA}^{-1}$ . Geometry optimization and time-dependent DFT (TD-DFT) calculations for  $[\text{Ni}(\text{Me}_3\text{-TACN})(\text{Cl})]^+$  were performed with the Gaussian 09 package.

## Reference

- [1] H. D. Kaesz and R. B. Saillant. "HYDRIDE COMPLEXES OF THE TRANSITION METALS" *Chem. Rev.*, 72, 1972, pp. 231–281.
- [2] S. Chakraborty, J. Zhang, J. A. Krause and H. Guan. "An Efficient Nickel Catalyst for the Reduction of Carbon Dioxide with a Borane" *J. Am. Chem. Soc.*, 132, 2010, pp. 8872–8873.
- [3] H. W. Lee, J. B. Ahn, J. H. Lee, S. K. Kang, S. K. Ahn and S. J. Lee. "Selective Reduction of Nitrocinnamoylfumagillols with  $\alpha,\beta$ -Unsaturated Ester Using Borohydride Exchange Resin (BER)-Nickel Acetate" *Heterocycles*, 65, 2005, pp. 1843–1856.
- [4] S. Yakabe, M. Hirano and T. Morimoto. "Hydrogenation of alkenes with sodium borohydride and moist alumina catalyzed by nickel chloride" *Tetrahedron Lett.*, 41, 2000, pp. 6795–6798.
- [5] D. Linden T. B. Reddy, *Handbook of Batteries*, McGraw-Hill, New York, 2002. pp. 1.3-43
- [6] U. Häussermann, H. Blomqvist and D. Noréus. "Bonding and Stability of the Hydrogen Storage Material  $Mg_2NiH_4$ " *Inorg. Chem.*, 41, 2002, pp. 3684–3692.
- [7] S. W. Ragsdale "Nickel-based Enzyme Systems" *J. Biol. Chem.*, 284, 2009, pp. 18571–18575.
- [8] A. Sigel, H. Sigel and R. K. O. Sigel. *Nickel and Its Surprising Impact in Nature*, John Wiley & Sons, Ltd, United Kingdom, 2007, ch. 7, vol. 2, pp. 279–322.
- [9] P. M. Vignais and B. Billou. "Occurrence, Classification, and Biological Function of Hydrogenases: An Overview", *Chem. Rev.*, 107, 2007, pp. 4206–4272.
- [10] T. A. Bobik, K. D. Olson, K. M. Noll and R. S. Wolfe. "Evidence that heterodisulfide of

coenzyme M and 7-mercaptoheptanoylthreonine phosphate is a product of the methylreductase reaction in methanobacterium” *Biochem. Biophys. Res. Commun.*, 149(2), 1987, pp. 455–460.

[11] J. Ellermann, R. Hedderich, R. Böcher and R. K. Thauer. “The final step in methane formation Investigations with highly purified methyl-CoM reductase (component C) from *Methanobacterium thermoautotrophicum* (strain Marburg)” *Eur. J. Biochem.*, 172, 1998, pp. 669–677.

[12] C. Holliger, G. Schraa, E. Stupperich, A. J. M. Stams and A. J. B. Zehnder. “Evidence for the Involvement of Corrinoids and Factor F<sub>430</sub> in the Reductive Dechlorination of 1,2-Dichloroethane by *Methanosarcina barkeri*” *Journal of Bacteriology*, 174(13), 1992, pp. 4427–4434.

[13] C. Holliger, S. W. M. Kengen, G. Schraa, A. J. M. Stams and A. J. B. Zehnder. “Methyl-Coenzyme M Reductase of *Methanobacterium thermoautotrophicum*  $\Delta H$  Catalyzes the Reductive Dechlorination of 1,2-Dichloroethane to Ethylene and Chloroethane” *Journal of Bacteriology*, 174(13), 1992, pp.4435–4443.

[14] B. Ganem and J. O. Osby. “Synthetically Useful Reactions with Metal Boride and Aluminide Catalysts” *Chem. Rev.*, 86, 1986, pp. 763–780.

[15] T. J. Marks and J. R. Kolb. “Covalent Transition Metal, Lanthanide, and Actinide Tetrahydroborate Complexes” *Chem. Rev.*, 77, 1977, pp. 263–293.

[16] P. J. Desrochers, S. Lelievre, R. J. Johnson, B. T. Lamb, A. L. Phelps, A. W. Cordes, W. Gu and S. P. Cramer. “A Stable Monomeric Nickel Borohydride” *Inorg. Chem.*, 42, 2003, pp.7945–7950.

[17] S. Chakraborty, J. Zhang, Y. J. Patel, J. A. Krause and H. Guan. “Pincer-Ligated Nickel Hydridoborate Complexes: the Dormant Species in Catalytic Reduction of Carbon Dioxide with Boranes” *Inorg. Chem.*, 52, 2013, pp. 37–47.

- [18] S. Murugesan, B. Stöger, M. Weil, L. F. Veiros and K. Kirchner “Synthesis, Structure, and Reactivity of Co(II) and Ni(II) PCP Pincer Borohydride Complexes” *Organometallics*, 34, 2015, pp.1364–1372.
- [19] M. Kandiah, G. S. McGrady, A. Decken and P. Sirsch. “[TriphosNi( $\eta^2$ -BH<sub>4</sub>)]: An Unusual Nickel(I) Borohydride Complex” *Inorg. Chem.*, 44, 2005, pp. 8650–8652.
- [20] A. J. Churchard, M. K. Cyranski, Ł. Dobrzycki, A. Budzianowski and W. Grochala. “Nickel macrocycles with complex hydrides—new avenues for hydrogen storage research” *Energy Environ. Sci.*, 3, 2010, pp. 1973–1978.
- [21] D. F. Evans and D. A. Jakubovic “Water-soluble Hexadentate Schiff-base Ligands as Sequestering Agents for Iron(III) and Gallium(III)” *J. Chem. Soc., Dalton Trans.*, 1988, pp. 2927–2933.
- [22] J. Cho, Y. M. Lee, S. Y. Kim and W. Nam. “Synthesis and crystal structure of nickel(II) complexes with bis(5-methyl-2-thiophenemethyl)(2-pyridylmethyl)amine” *Polyhedron*, 29, 2010, pp. 446–450.
- [23] F. A. Cotton, G. Wilkinson, C. A. Murillo and M. Bochmann, *Advanced Inorganic Chemistry*, Wiley, New York, 1999.
- [24] M. Cha, C. L. Gatlin, S. C. Critchlow and J. A. Kovacs. “Probing the Influence of Local Coordination Environment on Ligand Binding in Nickel Hydrogenase Model Complexes” *Inorg. Chem.*, 32, 1993, pp. 5868–5877.
- [25] J. D. Crane. “Bioinorganic chemistry” *Annu. Rep. Prog. Chem., Sect. A: Inorg. Chem.*, 93, 1997, pp. 593–610.
- [26] G. R. Fulmer, A. J. M. Miller, N. H. Sherden, H. E. Gottlieb, A. Nudelman, B. M. Stoltz, J. E. Bercaw and K. I. Goldberg. “NMR Chemical Shifts of Trace Impurities: Common Laboratory Solvents, Organics, and Gases in Deuterated Solvents Relevant to the

Organometallic Chemist” *Organometallics*, 29, 2010, pp. 2176–2179.

[27] P. J. Desrochers, J. Telser, S. A. Zvyagin, A. Ozarowski, J. Krzystek and D. A. Vivic. “Electronic Structure of Four-Coordinate  $C_{3v}$  Nickel(II) Scorpionate Complexes: Investigation by High-Frequency and -Field Electron Paramagnetic Resonance and Electronic Absorption Spectroscopies” *Inorg. Chem.*, 45, 2006, pp. 8930–8941.

[28] T. Deb, C. M. Anderson, H. Ma, J. L. Petersen, V. G. Young Jr. and M. P. Jensen. “Scorpionato Halide Complexes  $[(Tp^{Ph,Me})Ni-X]$  [ $X = Cl, Br, I; Tp^{Ph,Me} = \text{Hydrotris}(3\text{-phenyl-}5\text{-methyl-}1\text{-pyrazolyl})\text{-borate}$ ]: Structures, Spectroscopy, and Pyrazole Adducts” *Eur. J. Inorg. Chem.*, 2015, pp. 458–467.

[29] A. D. Becke. “Density-functional thermochemistry. III. The role of exact exchange” *J. Chem. Phys.*, 98, 1993, pp. 5648–5652.

[30] W. L. F. Armarego and D. D. Perrin, *Purification of Laboratory Chemicals*, Elsevier, Oxford, 1997.

[31] D. F. Evans “The Determination of the Paramagnetic Susceptibility of Substances in Solution by Nuclear Magnetic Resonance.” *J. Chem. Soc.*, 1959, pp. 2003–2005.

[32] J. Löliger and R. Scheffold. “Paramagnetic Moment Measurements by NMR A micro technique” *J. Chem. Educ.*, 49, 1972, pp. 646–647.

[33] G. M. Sheldrick, SHELXTL, Version 6.12, Bruker AXS, Inc., Madison, WI, 2001.

[34] P. B. Blöchl. “Projector augmented-wave method” *Phys. Rev. B: Condens. Matter*, 50, 1994, pp. 17953–17979.

[35] G. Kresse and J. Furthmüller. “Efficient iterative schemes for *ab initio* total-energy calculations using a plane-wave basis set” *Phys. Rev. B: Condens. Matter Mater. Phys.*, 54, 1996, pp. 11169–11186.

[36] G. Kresse and D. Joubert. “From ultrasoft pseudopotentials to the projector augmented-

wave method” *Phys. Rev. B: Condens. Matter Mater. Phys.*, 59, 1999, pp. 1758–1775.

## 요 약 문

본 논문은 니켈 보로하이드라이드 착물 및 이를 사용한 할로겐화 탄소의 탈할로겐화에 관한 것이다. 니켈(nickel)과 수소(hydrogen) 사이의 상호작용은 공업적 및 생물학적 촉매 시스템 분야에 있어 매우 중요하다. 니켈-수소 착물은 유기합성을 위한 촉매 수소화 반응, 재충전 전지를 위한 니켈 수소 배터리 및 수송을 위한 수소 저장과 밀접하게 관련되어 있다. 수소 가스로 양자(proton)의 두 개의 전자를 가역적으로 환원시키는 반응에 대하여 촉매로서 작용하는 수소화효소(hydrogenases) 등, 니켈을 함유하는 효소에 있어서 니켈-수소 부가물(adducts)은 효소 반응의 메커니즘에 있어서 매우 중요한 중간체이다. 현재, 니켈-수소 부가물에서 니켈-보로하이드라이드 종(species)이 관심이 높아지고 있으며 그 이유로는, 상기 니켈-수소 부가물이 니켈 촉매화된 수소첨가 반응(nickel-catalyzed hydrogenation)을 위한 잠재적인 물질이기 때문이다.

본 논문의 니켈-보로하이드라이드 화합물은 세자리 N-도너(donor) 리간드를 취하는 단핵의 고스핀 ( $\eta^2$ -BH<sub>4</sub>)니켈(II) 착물로서 CHCl<sub>3</sub> 등의 할로겐화 탄소에 대하여 탈할로겐 반응을 유도하는 현저한 효과가 있음을 확인하였다. 물과 토양의 치명적인 오염원인 할로겐화합물들은 인간과 동물에게 신경학적, 생식적인 독성을 가진다. 이런 할로겐물질의 분해를 통해 앞서 언급한 수소발생과 환경의 정화에 활용 될 수 있다는 점에서 의의를 가진다.

**핵심어 : 고스핀 니켈-보로하이드라이드 화합물, 탈할로겐반응**